Journal of Power Sources 196 (2011) 5990–5996

Contents lists available at ScienceDirect

Journal of Power Sources

journal homepage: www.elsevier.com/locate/jpowsour

Enhanced capacitance and rate capability of graphene/polypyrrole composite as electrode material for supercapacitors

Dacheng Zhang[a,b], Xiong Zhang[a], Yao Chen[a,b], Peng Yu[a,b], Changhui Wang[a,b], Yanwei Ma[a,*]

[a] Institute of Electrical Engineering, Chinese Academy of Sciences, Beijing 100190, People's Republic of China
[b] Graduate University of Chinese Academy Sciences, Beijing 100049, People's Republic of China

ARTICLE INFO

Article history:
Received 22 December 2010
Received in revised form 22 February 2011
Accepted 23 February 2011
Available online 6 March 2011

Keywords:
Graphene nanosheet
Polypyrrole
Composite
Electrode material
Supercapacitors

ABSTRACT

Graphene and polypyrrole composite (PPy/GNS) is synthesized via in situ polymerization of pyrrole monomer in the presence of graphene under acid conditions. The structure and morphology of the composite are characterized by X-ray diffraction (XRD), Raman spectroscopy, Fourier transform infrared spectrometer (FTIR), X-rays photoelectron spectroscopy (XPS) and transmission electron microscope (TEM). It is found that a uniform composite is formed with polypyrrole being homogeneously surrounded by graphene nanosheets (GNS). The composite is a promising candidate for supercapacitors to have higher specific capacitance, better rate capability and cycling stability than those of pure polypyrrole. The specific capacitance of PPy/GNS composite based on the three-electrode cell configuration is as high as 482 F g^{-1} at a current density of 0.5 A g^{-1}. After 1000 cycles, the attenuation of the specific capacitance is less than 5%, indicating that composite has excellent cycling performance.

1. Introduction

With the challenges ahead, including reducing environmental pollution and dependence on fossil fuel energy, the great efforts to revitalize the energy industry bring with it a valuable opportunity for us to provide a more stable and secure energy resource. Among them, energy storage is a key technology to enable renewable energy source deployment, and greatly reduce wasted energy. Supercapacitors, the energy storage devices between secondary batteries and traditional capacitors, have attracted considerable attention over the past decades for higher power density, longer cycle life, lower of cost and better environmental friendliness than secondary battery. With the unique advantages, they have been widely utilized in portable electronics, collecting intermittent energy, mobile communications and electrical vehicles [1,2]. Energy storage mechanisms of supercapacitors predominately include two ways: electric double layer effects and pseudocapacitance [3,4]. Commonly, porous carbon materials are the electrodes of double-layer capacitors, while transition metal oxides and conducting polymers are corresponding to pseudocapacitors [5]. In order to exploit the potential of supercapacitors, many efforts have been devoted to studying the carbon materials [6,7] and conducting polymer such as polyaniline (PANI) [8,9], polypyrrole (PPy) [10], and polythiophene (PT) [11]. With the intrinsic electrical conductivity and high capacitance as reported [12], polypyrrole is a promising electrode material for supercapacitors with unusual doping/dedoping processes, lower of cost, and simple synthesis. However, it also exhibits poor stability and rate capability, which limit its wide application [13]. Carbon materials such as activated carbon (AC), mesoporous carbon (MC), and carbon nanotubes (CNTs) usually display good stability. Recently, Jurewicz et al. obtained higher specific capacitance supercapacitors from carbon nanotube/polypyrrole composites electrode than pure samples because of the synergistic effects between these components [14]. However, attractive CNTs are still very expensive and their double-layer capacitance is low [15,16].

More recently, graphene, a single atomic plane of graphite [17], is expected to be an excellent electrode material for supercapacitors due to its superior electrical conductivity, high specific surface area, and chemical stability. It has been demonstrated that graphene-based supercapacitors have high specific capacitance (135–264 F g^{-1}) [18–22]. More importantly, graphene can also be easily incorporated with conducting polymers as precursor [23–25] to improve the electrochemical properties of composite by the synergistic effects, because the ultrathin flexible graphene layers cannot only increase the conductivity of the composite, but also effectively improve the stability of the polymer during charge/discharge process. Yan et al. prepared a graphene/polyaniline composite by in situ polymerization with a high specific capacitance of 1046 F g^{-1} at a scan rate of 1 mV s^{-1} compared to 115 F g^{-1} for the pure PANI [23]. However, the capacitance was mainly dominated by the pseudocapacitance from

* Corresponding author. Tel.: +86 10 82547129; fax: +86 10 82547137.
E-mail address: ywma@mail.iee.ac.cn (Y. Ma).

0378-7753/$ – see front matter © 2011 Elsevier B.V. All rights reserved.
doi:10.1016/j.jpowsour.2011.02.090

the PANI. On this basis, Zhang et al. also developed another method to prepare the graphene/polyaniline composite, and the specific capacitance reached 480 F g^{-1} at a current density of 0.1 A g^{-1}. However, the specific capacitance retention at higher charge–discharge current densities (210 F g^{-1} at the current density of 1 A g^{-1}) and cycling stability of this composite should be improved [15]. Although some efforts have been made on the composite of graphene with conducting polymer, it is still a challenge to synthesize graphene/conducting polymer composite as electrode materials with the high capacitance and good rate performance for supercapacitors.

Herein, we report a facile strategy to synthesize graphene and PPy composite (PPy/GNS) using an in situ polymerization method. We also describe charge storage properties of the resulting composite in 1 M H_2SO_4 aqueous electrolyte. The high specific capacitance of 482 F g^{-1} is obtained from galvanostatic charge–discharge at a constant current density of 0.5 A g^{-1}, which is much larger than that of each pristine component. This composite not only achieves high specific capacitance properties of PPy, but also keeps the advantage of an excellent conductivity in the single layer network of graphene.

2. Experimental

2.1. Preparation of samples

All the chemicals were of analytical grade and were used without further purification. GNS was prepared by reduction of graphene oxide with hydrazine hydrate according to the literature [26]. Nanocomposite was synthesized using in situ polymerization in the presence of GNS suspension and pyrrole with different ingredient mass ratios from 9:1 to 5:5 for pyrrole and graphite oxide. The nanocomposite synthesized from different ratios is signed as PGratio. Here we take the $PG_{9:1}$ composite as an example, indicating that the mass ratio of pyrrole and graphite oxide is 9:1. Firstly, 0.45 g pyrrole monomers were added into 50 mL of 1 g L^{-1} graphene aqueous suspension and sonicated for 30 min. Then, an equal volume of 6.7 mM $FeCl_3$ solution (solvent: 0.1 M HCl) was slowly added into the above mixture and kept at 0–4 °C for 24 h. Finally, the reaction mixture was filtered, and washed with deionized water and ethanol, and then the product was dried at 60 °C for 24 h. For comparison, the pure polypyrrole was prepared without graphene by the similar procedure.

2.2. Characterization methods

X-ray diffraction (XRD) analyses were performed using a X' Pert Pro system with Cu Kα radiation (λ = 1.54060 Å) operated at 40 kV and 40 mA. Raman spectra were obtained on a RM 2000 microscopic confocal Raman spectrometer (Renishaw in Via Plus, England) employing a 514 nm laser beam. Fourier transform infrared spectroscopy (FTIR) spectra were measured using a Nicolet IR 750 spectrometer with pure KBr as the background. X-rays photoelectron spectroscopy (XPS) analysis was recorded on a PHI Quantear SXM (ULVAC-PH INC) which used Al as anode probe in 6.7×10^{-8} Pa. C, H and N microanalysis was recorded on an Elementar Vario El elemental analyzer. Transmission electron microscopy (TEM) and high resolution transmission electron microscopy (HRTEM) were carried out using a JEOL JSM-2010 operating at an accelerating voltage of 200 kV. Electronic conductivity was measured on compacted pellets by standard four-probe resistance using Physical Property Measurement System (PPMS).

2.3. Electrochemical measurements

The electrode performance was measured in a beaker-type electrochemical cell equipped with the working electrode, a platinum sheet as the counter electrode, and a standard calomel electrode (SCE) as the reference electrode. The working electrode was prepared by mixing 70 wt% active material, 20 wt% acetylene black, and 10 wt% poly(vinylidene fluoride) in N-methyl-2-pyrrolidone and the slurry was spread onto a titanium plate with 1 cm^2 geometry area. The electrode was heated at 120 °C for 2 h to evaporate solvent. The electrolyte was 1 M H_2SO_4.aqueous solution. Cyclic voltammetry (CV), galvanostatic charge–discharge and electrochemical impedance spectroscopy (EIS) were measured by a CHI 660C electrochemical workstation. CVs were carried out at the scan rates ranging from 2 to 500 mV s^{-1} within the potential range of −0.2 to 0.7 V (vs. SCE). Galvanostatic charge–discharge was carried out at current densities ranging from 0.5 to 5 A g^{-1}. EIS was recorded under the following condition: AC voltage amplitude 5 mV, frequency range from 0.1 to 10^5 Hz at 0.4 V.

3. Results and discussion

3.1. Structure and morphology studies

Fig. 1a shows the XRD patterns of GNS, pure PPy and PPy/GNS samples with different ingredient mass ratios. For GNS, the diffraction peaks at $2\theta = 24.5°$ and 42.8° can be attributed to the graphite-like structure (0 0 2) and (1 0 0), respectively. A characteristic peak of amorphous for pure PPy appears at about $2\theta = 26°$ [27]. As the GNS percentage increases in the composite, the broad peak also shifts from $2\theta = 26°$ to 24.8° and the peak at 42.8° does not obviously appear, implying that the PPy and GNS have been completely interacted. Here, we can calculate that the value of interplanar spacing is about 0.34 nm for the broad peak about at $2\theta = 25°$, which is identical to the π–π stacking distance. As a result, we can speculate that there probably exists π–π stacking between the PPy chains and the graphene planes, further supported by the HRTEM images [28]. Raman spectroscopy is as shown in Fig. 1b, which is widely used to obtain structural information about carbon-based materials. The Raman spectroscopy of all samples exist two prominent peaks at about 1590 and 1350 cm^{-1}, which correspond to the G and D bands, respectively (Fig. 1b). The G and D bands are significantly broadened with the introduction of GNS, suggesting that the nanocrystal size decreases due to the phonon confinement [29]. Additionally, there are a broad peak at 1051 cm^{-1} and two small peaks at 933 and 981 cm^{-1} for pure PPy and PGratio composite, which are the characteristic peaks of PPy.

The FTIR absorption spectra of the PPy and $PG_{9:1}$ are shown in Fig. 1c. From the top of spectrum, the characteristic polypyrrole peaks are located at 1529 cm^{-1} and 1446 cm^{-1}, which are due to the antisymmetric and symmetric ring-stretching modes, respectively [30]. Strong peaks near 1144 cm^{-1} and 887 cm^{-1} indicate the doping state of polypyrrole, and a broad band at 3000–3500 cm^{-1} describes N–H and C–H stretching vibrations. Furthermore, the bands at 1030 and 1284 cm^{-1} are attributed to C–H deformation vibrations and C–N stretching vibrations, respectively [31–33]. Compared with the pure PPy, it is clearly observed that most of the marked peaks are shifted left when the graphene was introduced into the synthesis process of PPy. This reveals that the groups from graphene are associated to the nitrogenous functional groups of PPy backbone via the same doping process into the PPy backbone, just as the normal dopant of Cl^- [34]. Herewith, there probably exist interactions such as π–π stacking between polypyrrole backbone and graphene or hydrogen bonding for the residual oxygen functional groups on graphene.

Similar phenomenon is also observed by N 1s XPS core-level spectra for $PG_{9:1}$. From Fig. 2, the peaks are reasonably decomposed into three Gaussian peaks with the binding energy of 398.2, 399.9 and 401.2 eV, respectively. The peak at 398.2 eV related to the neutral and the imine-like structure (>C═N–) can be used to

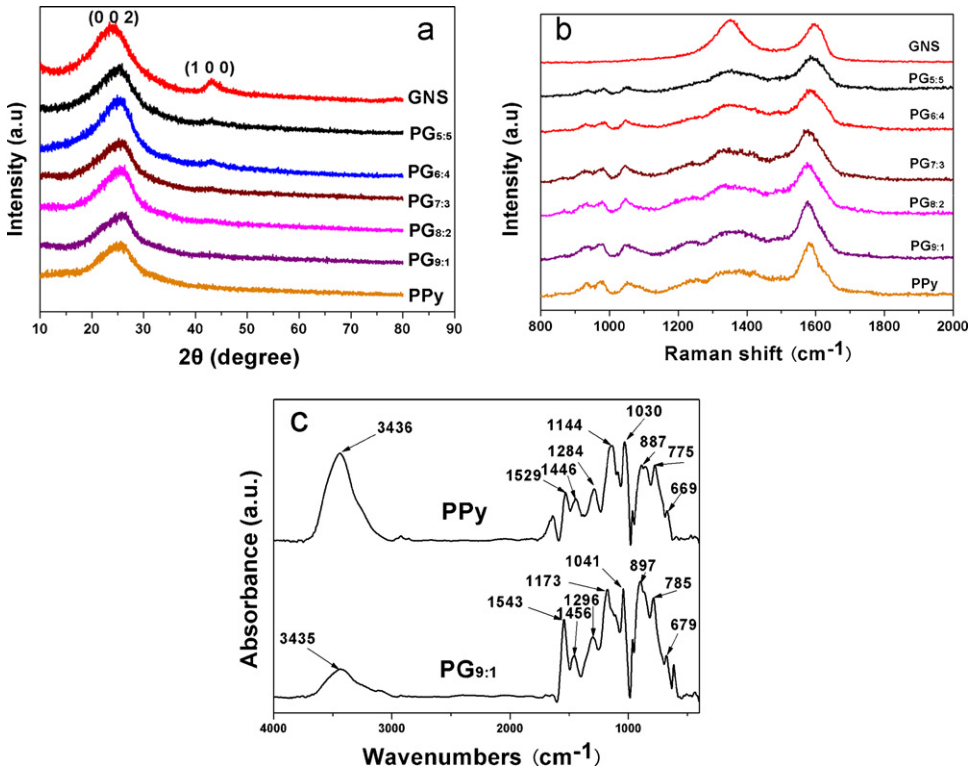

Fig. 1. (a) XRD patterns, (b) Raman spectra of PPy, GNS and PGratio. (c) FTIR spectra of the PPy and $PG_{9:1}$ composite.

estimate the density of defects within the PPy [35], because the structure is believed to interrupt the electron hopping on the polymer chain [36]. The peak at 399.9 eV is owing to the neutral and amine-like structure (–NH–) [37]. The peak at 401.2 eV is caused by the positively charged Nitrogen atoms with protonation ($–NH^+–$) [38]. Consequently, the doping level and the defect density of pure PPy and $PG_{9:1}$ composite can be quantitatively estimated. The former is calculated from the ratio of the area of peak at 401.2 eV to the total area of the N 1s peak, and the latter from the ratio of the 398.2 eV to the same area. The doping level of composite is increasing from 0.208 to 0.308 and the defect density is reducing from 0.013 to 0.0016 after the introduction of graphene. The higher doping level of composite is consistent with its higher electronic conductivity tests, showing that the conductivity of PPy and $PG_{9:1}$ composite are 107 S m^{-1} and 685 S m^{-1}, respectively. Moreover, the lower defect density and higher conductivity of the composite may make a contribution towards the higher capacitance and better rate capability.

TEM and HRTEM characterization are also used to investigate the structure and morphology of the samples. Fig. 3 shows TEM and HRTEM images of GNS, PPy and $PG_{9:1}$. The GNS is agglomerated into sheet structures with hundreds of nanometers and scrolled like crumpled paper, as shown in Fig. 3a. Meanwhile, the HRTEM image suggests that the GNS consists of less than a few orderly arranged carbon layers, indicated by arrows in Fig. 3b. Fig. 3c shows that pure polypyrrole has been synthesized like bulk with several of micrometers. The HRTEM image displays the amorphous structure of PPy (Fig. 3d). Compared with Fig. 3d, Fig. 3e demonstrates that the PPy has been homogeneously surrounded like an entangled state by GNS. Furthermore, the particle sizes of composite are obviously smaller than pure PPy as can be seen from Fig. 3c and e. The lattices (neighboring distance about 0.34 nm) and the amorphous structure of PPy are also found from Fig. 3f. Surprisingly, the number of lattices in $PG_{9:1}$ (only 6.7 wt% GNS estimated by C, H and N elemental analysis) is more than that of pure GNS, confirming that the graphene and polypyrrole are strongly incorporated by interactions such as π–π stacking. No matter the Raman or TEM image, the results show the particles are smaller than pure samples. In general, nanocrystallization of the material could lead to higher specific surface, high electrochemical utilization, and the

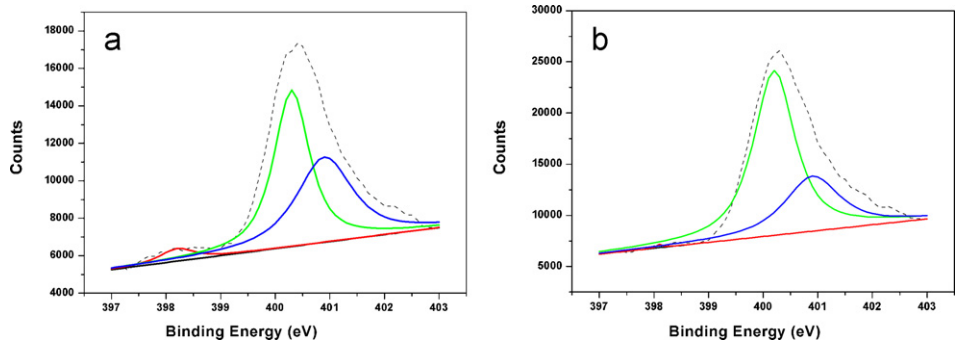

Fig. 2. (a) and (b) N 1s XPS core-level spectra of the PPy and $PG_{9:1}$ composite, respectively. Dashed line is the measure curve, and solid line is the fitting curve.

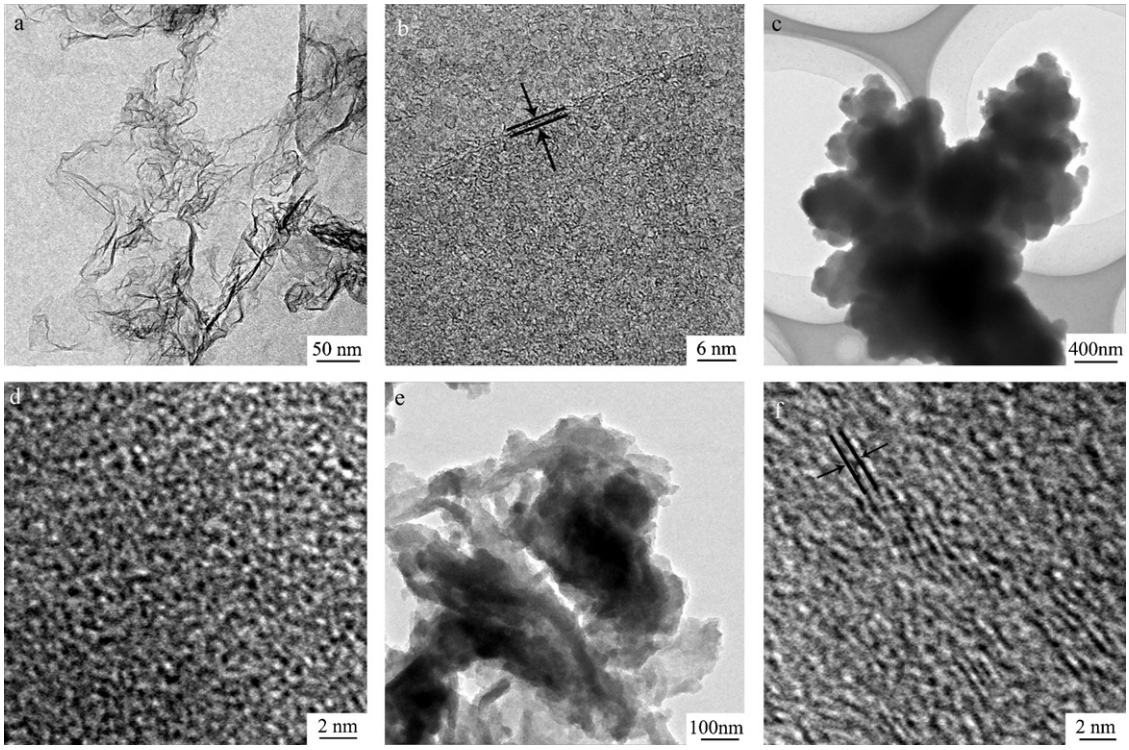

Fig. 3. (a) and (b) TEM and HRTEM images of GNS; (c) and (d) TEM and HRTEM images of PPy; (e) and (f) TEM and HRTEM images of $PG_{9:1}$.

enhancement of the electrochemical properties as electrodes for supercapacitors [39].

3.2. Electrochemical properties

The electrochemical performance of the samples as the electrode material for supercapacitors was tested by cyclic voltammetry (CV) and galvanostatic charge–discharge technique in three-electrode system. Fig. 4 exhibits the cyclic voltammetry of the $PG_{9:1}$ composite electrode with a potential range between −0.2 and 0.7 V (vs. SCE) at different scan rates from 5 to 500 mV s^{-1}. The shapes of all CV curves show the rectangular and symmetric current–potential characteristics, meaning the ideal capacitive behavior. In addition, it is also seen that there are no clear redox peaks in the potential range between −0.2 and 0.7 V (vs. SCE). The rectangular shape can remain even at a very high scan rate of 500 mV s^{-1}, indicative of highly capacitive nature with good ion response.

Fig. 5a and b shows the galvanostatic charge–discharge curves of PPy, GNS, and $PG_{9:1}$ electrodes at current densities of 0.2 and 5 A g^{-1}, respectively. Fig. 5a and b presents that the capacitive behavior of the composite is also very good because of the near triangle shape. The specific capacitance of the composite is higher than that of pure PPy and GNS under the same current density which can be clearly found from the specific capacitance curves (Fig. 5c). The specific capacitance of the electrode using galvanostatic can be calculated according to the following Eq. (1):

$$C = \frac{1 \times \Delta t}{m \times \Delta V} \quad (1)$$

where I is the current, ΔV is the potential window, Δt is the discharge time, m is the mass of active material in a single electrode.

As shown in Fig. 5c, the specific capacitance of the $PG_{7:3}$ is the highest (482 F g^{-1}, 0.5 A g^{-1}) among all the samples, which exceeds that of pure polypyrrole (152 F g^{-1}), and remains 222 F g^{-1} at the current density of 5 A g^{-1}, while that of pure polypyrrole sharply decreases to only 43 F g^{-1}. It is noted that the $PG_{6:4}$ composite shows not only high capacitance but also better rate capability, indicating this ratio is optimal among all the samples. Based on the discussion above, the improved capacitance and better rate

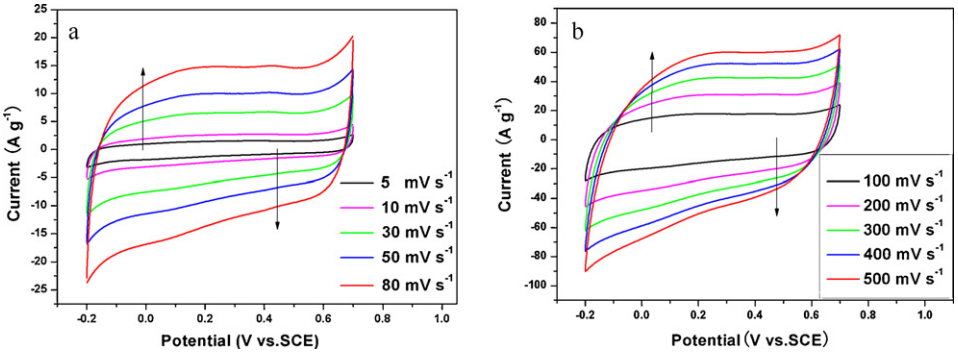

Fig. 4. (a) and (b) CVs of $PG_{9:1}$ composite at various scan rates with potential from −0.2 to 0.7 V (vs. SCE). The total mass of active material of electrode is about 0.4 mg (1 cm^2) with the thickness of 30 μm for all electrodes in three-electrode system.

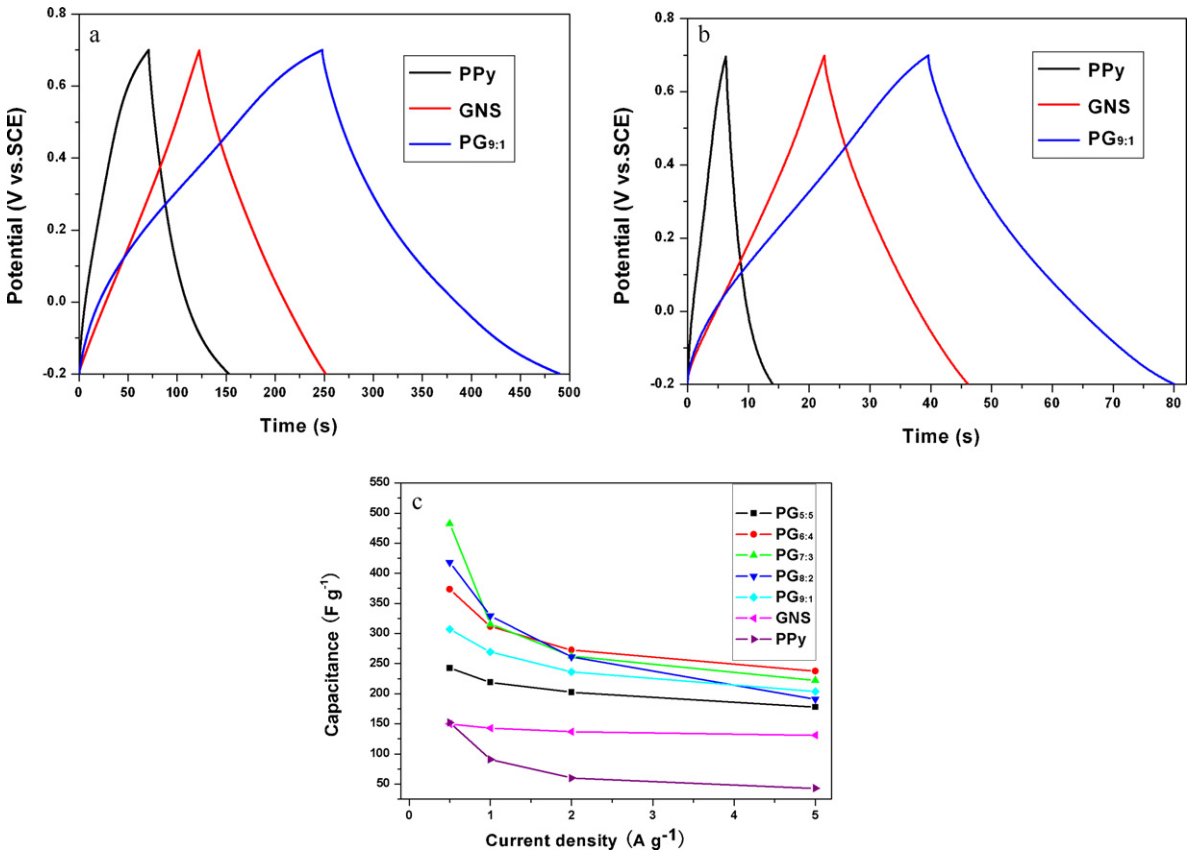

Fig. 5. (a) and (b) Galvanostatic charge–discharge curves of PPy, GNS and $PG_{9:1}$ at current densities of 0.2 and 5 A g^{-1}, respectively. (c) The specific capacitances of PPy, GNS and PGratio electrodes at different current densities.

capability of composite might be mainly ascribed to higher conductivity and smaller particle sizes of composite, which can shorten ion diffusion length and make higher materials utilization.

Fig. 6 shows the complex plane impedance plots produced from EIS analyses of the PPy, GNS and $PG_{9:1}$ electrode. The equivalent series resistance (ESR) of all the materials is about 1 Ω, which is the intercept of the plot with the real impedance (Z'), including both the solution resistance and the DC resistance [40]. The impedance plot shown in Fig. 6 can be divided into the high-frequency and the low-frequency component of the plot. The semicircle at the high frequency is nearly not detected for all electrodes, suggesting that interfacial charge-transfer resistance is significantly low or body impedance is too large. The 45° sloped portion of the Nyquist plots in the low frequency is the Warburg resistance resulting from the frequency dependence of ion diffusion/transport in the electrolyte. The larger Warburg resistance indicates greater variations in ion diffusion path lengths and increases obstruction of ion movement. The slope of the impedance plots of GNS (nearly vertical) and $PG_{9:1}$ increases obviously in the low frequency, while that of PPy always stays almost constant. The reduced resistance of the composite may be in part due to the network of the graphene structure, which facilitates the efficient access of electrolyte ions to the graphene surface and shortens the ion diffusion path. In addition, it suggests that GNS shows better capacitive than PPy [41].

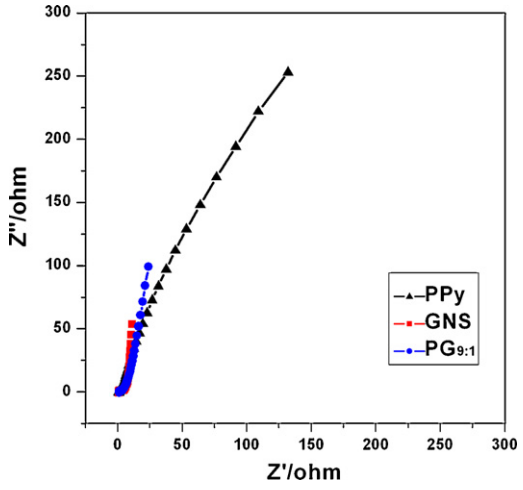

Fig. 6. Nyquist impedance plots of the PPy, GNS and $PG_{9:1}$ electrodes.

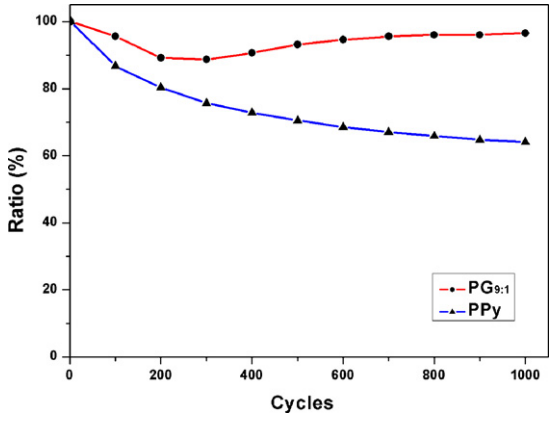

Fig. 7. Capacitance retention ratio of PPy and $PG_{9:1}$ electrodes from the 1st to the 1000th cycle at the scan rate of 50 mV s^{-1}.

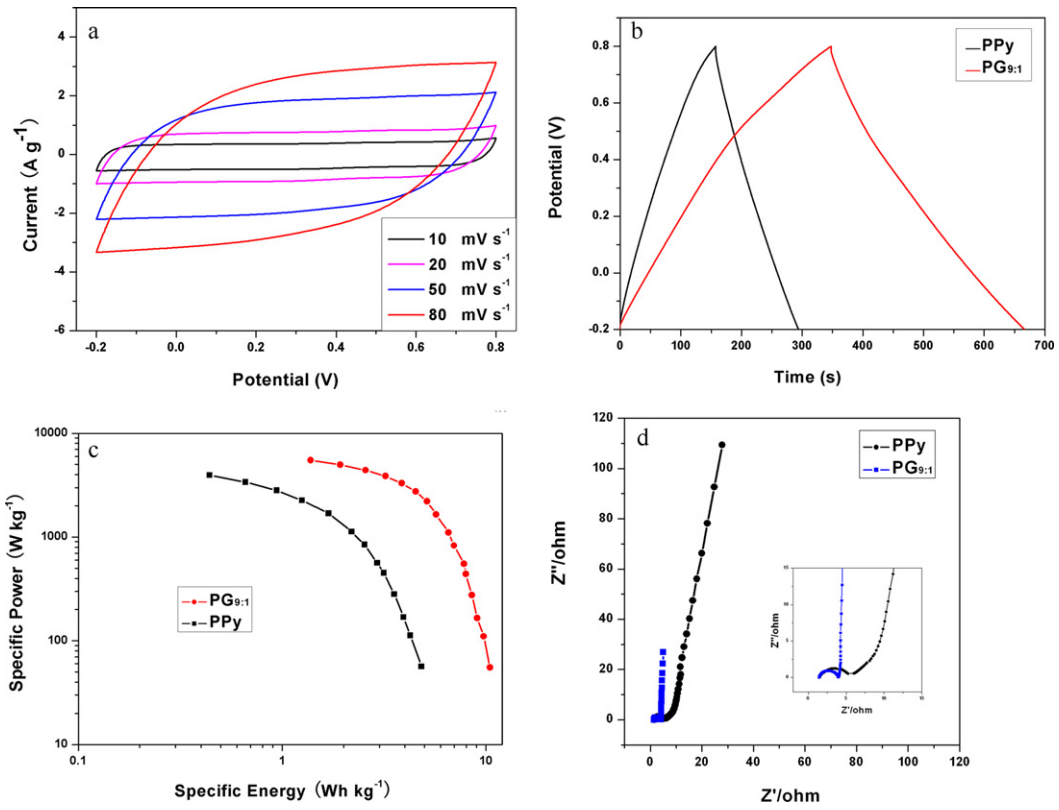

Fig. 8. (a) CVs of $PG_{9:1}$ composite as a two-electrode cell configuration at various scan rates with the potential from −0.2 V to 0.8 V in 1 M H_2SO_4. (b) Galvanostatic charge–discharge curves of PPy and $PG_{9:1}$ composite at the current of 2 mA. (c) Ragon plots of PPy and $PG_{9:1}$. (d) Nyquist impedance plots of the PPy and $PG_{9:1}$; The total mass of active material of two electrodes is 9.1 mg.

Fig. 7 shows the cyclic stability of the $PG_{9:1}$ and pure PPy electrodes at the scan rate of 50 mV s^{-1}. There are a decrease in the first 200 cycles and thereafter an increase for the specific capacitance of $PG_{9:1}$. The increase of the specific capacitance is maybe due to that the oxygen groups on the graphene are further reduced by electrochemical reaction, which is consistent with other report [42]. Besides, the activation of electrode material also leads to higher conductivity because of better contact between electrolyte and electrode material. After 1000 cycles, the specific capacitance keeps 96% for $PG_{9:1}$, while just only 64% for PPy. This obviously enhanced cyclic stability for $PG_{9:1}$ composite is resulted from graphene which can stabilize the structure of PPy during the charge–discharge processes.

To further estimate the actual performance of composite as electrode material for supercapacitors, we have also fabricated the symmetric two-electrode cell. Fig. 8a and b shows that the curves also nearly stay rectangle and triangle through cyclic voltammetry and galvanostatic charge–discharge tests. The specific capacitance of single electrode is 280 F g^{-1} at the current density of 2 mA with a wider potential window (−0.2 to 0.8 V). In addition, the specific energy and specific power of the $PG_{9:1}$ composite are also considerable. The specific energy and specific power of the samples in two-electrode system are estimated from galvanostatic discharge curves at the different currents and marked in the Ragon plot, as shown in Fig. 8c. The specific energy values of $PG_{9:1}$ electrode are in the range of 1.4–10.5 Wh kg^{-1}, while the specific power values are in the range of 55–5510 W kg^{-1}, revealing that there is a decrease in specific energy of the electrode material with an increase of specific power. The specific energy values of PPy electrode are in the range of 0.5–4.8 Wh kg^{-1}, while the specific power values are in the range of 55–3950 W kg^{-1}. Compared with $PG_{9:1}$ and pure PPy electrodes, the specific energy of $PG_{9:1}$ is much higher than pure PPy under the same specific power. The maximum power density can be calculated according to the following Eq. (2):

$$P_{\max} = \frac{U_0^2}{4mR} \tag{2}$$

where U_0 is the potential at the beginning of discharge, R is the ESR, and m is the total mass of active material of the two electrodes [43]. The ESR as shown in Fig. 8d is only 1.39 Ω for the $PG_{9:1}$ electrode, and the maximum power density $P_{\max}$ = 12.7 kW kg^{-1} is obtained. The good electrochemical properties of the $PG_{9:1}$ composite might be ascribed to nanocrystallization of the composite and the enhanced conductivity of the whole electrode.

4. Conclusions

Composite of graphene and polypyrrole was synthesized via in situ polymerization, showing higher specific capacitance, better rate capability and cycling stability as supercapacitor electrodes. Studies of structural and morphological reveal that it is probably due to interactions between polypyrrole and graphene during the in situ polymerization, such as hydrogen bonding and π–π stacking. The nanostructure of the PPy was induced and greatly affected by the addition of graphene during the synthesis process, which might greatly contribute to the electrochemical properties of the composite. With a small content of graphene (6.7 wt% in $PG_{9:1}$) in the composite, not only the specific capacitance but its rate capability is also enhanced. Further optimization and control of the structures to exploit better electrochemical properties of graphene-based composites are under investigation in our group.

Acknowledgements

This work was partially supported by the Knowledge Innovation Program of the Chinese Academy of Sciences (No. KJCX2-YW-W26), the National Natural Science Foundation of China (Nos. 21001103 and 51025726) and the Director Foundation of Institute of Electrical Engineering.

References

[1] M. Winter, R.J. Brodd, Chem. Rev. 104 (2004) 4245–4269.
[2] F. Lufrano, P. Staiti, Electrochim. Acta 49 (2004) 2683–2689.
[3] B.E. Conway, Electrochemical Supercapacitors, Scientific Fundamentals and Technological Applications, Kluwer Academic/Plenum Press, New York, 1999.
[4] K.W. Nam, K.B. Kim, J. Electrochem. Soc. 149 (2002) A346–A354.
[5] B.E. Conway, W.G. Pell, J. Solid State Electrochem. 7 (2003) 637–644.
[6] X. Zhao, H. Tian, M.Y. Zhu, K. Tian, J.J. Wang, F.Y. Kang, R.A. Outlaw, J. Power Sources 194 (2009) 1208–1212.
[7] Y.P. Zhang, H.B. Li, L.K. Pan, T. Lu, Z. Sun, J. Electroanal. Chem. 634 (2009) 68–71.
[8] D.S. Dhawale, D.P. Dubal, V.S. Jamadade, R.R. Salunkhe, C.D. Lokhande, Synth. Met. 160 (2010) 519–522.
[9] X. Zhang, L.Y. Ji, S.C. Zhang, W.S. Yang, J. Power Sources 173 (2007) 1017–1023.
[10] K.A. Noha, D.W. Kim, C.S. Jin, K.H. Shin, J.H. Kim, J.M. Ko, J. Power Sources 124 (2003) 593–595.
[11] A. Laforgue, P. Simon, C. Sarrazin, J.F. Fauvarque, J. Power Sources 80 (1999) 142–148.
[12] J. Wang, Y.L. Xu, X. Chen, X.F. Du, J. Power Sources 163 (2007) 1120–1125.
[13] X. Zhang, W.S. Yang, Y.W. Ma, Electrochem. Solid State Lett. 12 (2009) A95–A98.
[14] Frackowiak, V. Khomenko, K. Jurewicz, K. Lota, F. Beguin, J. Power Sources 153 (2006) 413–418.
[15] K. Zhang, L.L. Zhang, X.S. Zhao, J.S. Wu, Chem. Mater. 22 (2010) 1392–1401.
[16] R.R. Bi, X.L. Wu, F.F. Cao, L.Y. Jiang, Y.G. Guo, L.J. Wan, J. Phys. Chem. C 114 (2010) 2448–2541.
[17] A.K. Geim, Science 324 (2009) 1530–1534.
[18] W. Lv, D.M. Tang, Y.B. He, C.H. You, Z.Q. Shi, X.C. Chen, C.M. Chen, P.X. Hou, C. Liu, Q.H. Yang, ACS Nano 3 (2009) 3730–3736.
[19] M.D. Stoller, S. Park, Y. Zhu, J. An, R.S. Ruoff, Nano Lett. 8 (2008) 3498–3502.
[20] Y. Zhu, S. Murali, M.D. Stoller, A. Velamakanni, R.D. Piner, R.S. Ruoff, Carbon 48 (2010) 2118–2122.
[21] X. Du, P. Guo, H. Song, X. Chen, Electrochim. Acta 55 (2010) 4812–4819.
[22] Y. Chen, X. Zhang, P. Yu, Y.W. Ma, J. Power Sources 195 (2010) 3031–3035.
[23] J. Yan, T. Wei, B. Shao, Z.J. Fan, W.Z. Qian, M.L. Zhang, F. Wei, Carbon 48 (2010) 487–493.
[24] Q. Wu, Y.X. Xu, Z.Y. Yao, A.R. Liu, G.Q. Shi, ACS Nano 4 (2010) 1963–1970.
[25] D.W. Wang, F. Li, J.P. Zhao, W.C. Ren, Z.G. Chen, J. Tan, Z.S. Wu, I. Gentle, G.Q. Lu, H.M. Cheng, ACS Nano 3 (2009) 1745–1752.
[26] D. Li, M.B. Muller, S. Gilje, R.B. Kaner, G.G. Wallace, Nat. Nanotechnol. 3 (2008) 101–105.
[27] T. Vishnuvardhan, V. Kulkarni, C. Basavaraja, S. Raghavendra, Bull. Mater. Sci. 29 (2006) 77–83.
[28] J. Lee, S. Cho, S. Park, J. Kim, J. Yu, Y. Kim, T. Russell, Nano Lett. 8 (2008) 2315–2320.
[29] D. Bersani, P.P. Lottici, X.Z. Ding, Appl. Phys. Lett. 72 (1998) 73–75.
[30] G. Cho, B.M. Fung, D.T. Glatzhofer, J.S. Lee, Y.G. Shul, Langmuir 17 (2001) 456–461.
[31] B. Tian, G. Zerbi, J. Chem. Phys. 92 (1990) 3886–3891.
[32] H.N.M.E. Mahmud, A. Kassim, Z. Zainal, W.M.M. Yunus, J. Appl. Polym. Sci. 100 (2006) 4107–4113.
[33] X.T. Zhang, J. Zhang, Z.F. Liu, C. Robinsonb, Chem. Commun. (2004) 1852–1853.
[34] H.L. Wang, Q.L. Hao, X.J. Yang, L.D. Lu, X. Wang, Electrochem. Commun. 11 (2009) 1158–1161.
[35] J. Joo, J.K. Lee, S.Y. Lee, K.S. Jang, E.J. Oh, A.J. Epstein, Macromolecules 33 (2000) 5131–5136.
[36] J.M. Ribo, A. Dicko, J.M. Tura, D. Bloor, Polymer 32 (1991) 728–732.
[37] E.T. Kang, K.G. Neoh, Y.K. Ong, K.L. Tan, B.T. Tan, Macromolecules 24 (1999) 2822–2828.
[38] D.B. Cairns, S.P. Armes, M.M. Chehimi, C. Perruchot, M. Delamar, Langmuir 15 (1999) 8059–8066.
[39] E. Machefaux, T. Brousse, D. Belanger, D. Guyomard, J. Power Sources 165 (2007) 651–655.
[40] R.P. Ramasamy, B. Veeraraghavan, B. Haran, B.N. Popov, J. Power Sources 124 (2003) 197–203.
[41] Q.F. Wu, K.X. He, H.Y. Mi, X.G. Zhang, Mater. Chem. Phys. 101 (2007) 367–371.
[42] Y.Y. Shao, J. Wang, M. Engelhard, C.M. Wang, Y.H. Lin, J. Mater. Chem. 20 (2010) 743–748.
[43] Y. Wang, Z.Q. Shi, Y. Huang, Y.F. Ma, C.Y. Wang, M.M. Chen, Y.S. Chen, J. Phys. Chem. C 113 (2009) 13103–13107.